Incommensurate Spin Density Waves in Iron Aluminides

D. R. Noakes,[1] A. S. Arrott,[1,2] M. G. Belk,[1] S. C. Deevi,[3] Q. Z. Huang,[4] J. W. Lynn,[4] R. D. Shull,[2] and D. Wu[5]

[1]*Center for Interactive Micromagnetics, Virginia State University, Petersburg, Virginia 23806, USA*
[2]*MSEL, National Institute of Standards and Technology, Gaithersburg, Maryland 20899, USA*
[3]*Research, Development and Engineering Center, Philip Morris USA, Richmond, Virginia 23261, USA*
[4]*NCNR, National Institute of Standards and Technology, Gaithersburg, Maryland 20899, USA*
[5]*Thayer School of Engineering, Dartmouth College, Hanover, New Hampshire 03755, USA*

(Received 5 August 2003; published 18 November 2003)

Neutron diffraction in Fe(Al) reveals incommensurate spin density waves (SDWs) in alloys known to be spin glasses. The wave vectors for crystals of Fe(34Al), Fe(40Al), and Fe(43Al) show n varying from 11 to 6 for $\vec{q} = 2\pi(h \pm 1/n, k \pm 1/n, l \pm 1/n)/a_0$, where (h, k, l) and a_0 characterize the parent bcc lattice of the CsCl structure. The magnetic reflections are present far above the spin-glass freezing temperatures. These SDWs keep the spins on nearest-neighbor Fe atoms close to parallel, in contrast with SDWs in Cr, which keep nearest-neighbor spins close to antiparallel.

DOI: 10.1103/PhysRevLett.91.217201 PACS numbers: 75.25.+z, 75.30.Fv, 75.50.Bb

We report neutron diffraction results showing antiferromagnetic order in iron aluminides. The structure could be generated by a set of spin density waves (SDWs) with wave vectors $\vec{q} = 2\pi(\pm\frac{1}{n}, \pm\frac{1}{n}, \pm\frac{1}{n})/a_0$, where a_0 is the lattice parameter of the parent bcc lattice underlying the B2(CsCl) structure of the atomically ordered iron aluminides, Fe(22Al) to Fe(55Al). The denominator n takes values from 11 to 6 as the concentration of Al is increased from Fe(34Al) to Fe(43Al). The continuous variation of n with concentration and temperature shows the wave vectors are incommensurate with the lattice.

Iron aluminides have been the focus of recent discussions of the limits to density functional theory in the local spin density approximation [1,2]. We present arguments that affirm the statement "SDWs and antiferromagnetism are complex subjects with pervasive ramifications in condensed-matter physics" [3].

In 1958, Sato and Arrott predicted an antiferromagetic state for these compositions [4]. By 1980, probably everyone, including them, became convinced that this system is best described by the term *spin glass,* for, indeed, these alloys have all the properties associated with that term; see Shapiro [5]. Peaks in the temperature dependence of the magnetic susceptibility that signal the onset of spin-glass freezing have been observed [6–8].

A dramatic transition from paramagnetism to ferromagnetism back to paramagnetism with decreasing temperature occurs for Fe(30.5Al). The inverse Curie temperature is 180 K. A "spin-glass state" appears below 80 K. Sato and Arrott attributed this behavior to competition between nearest neighbors with ferromagnetic (FM) coupling and third neighbors with antiferromagnetic (AFM) coupling, where the Fe(I) atoms on opposite cube corners interact by a 180° superexchange when the center site of the bcc cube is occupied by an Al atom. Their predicted long-range antiferromagetism was not seen in neutron diffraction studies of their Fe(Al) alloys [9] nor in detailed studies of Fe(30.5Al) [10,11].

The CsCl structure naturally divides into two simple cubic lattice complexes, one filled by Fe(I) atoms while the predominantly Al sublattice has the remaining Fe(II) atoms occupying sites at random, leading to frustration of the spin system in trying to resolve the competition between the two interactions.

In Fe_3Al the Al sublattice itself becomes ordered, breaking into two fcc lattice complexes; one is filled by Fe(II) and the other by Al. The symmetry is DO_3. The material is ferromagnetic, but, as noted by Grest [12], if the 180° superexchange interaction were stronger, Fe_3Al would have the AFM state shown in Fig. 1(a), corresponding to wave vectors $\vec{q} = 2\pi(\pm\frac{1}{4}, \pm\frac{1}{4}, \pm\frac{1}{4})/a_0$. Figure 1(b) applies to hypothetical Fe_9Al_7 [2], where the nodes of the SDW pattern are at the positions of the Al atoms and the antinodes center on the clusters of nine Fe atoms.

The change in structural unit cell from fcc in Fig. 1(a) to primitive cubic in Fig. 1(b) frees the cube of Fe(I) atoms to adjust its positions with respect to the Al atoms, changing the volumes of Fe atoms and affecting their

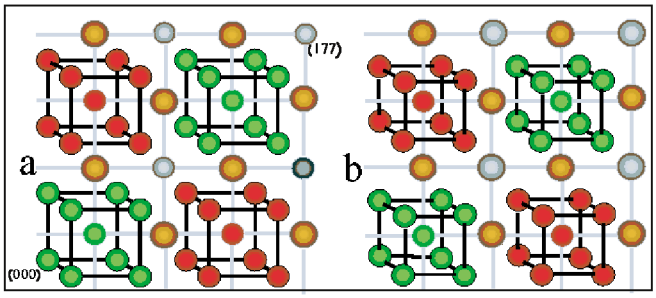

FIG. 1 (color). Magnetization patterns with cubic symmetry for (a) Fe_3Al and (b) Fe_9Al_7. The green and red atoms are Fe(I) sites with opposite spin directions. The gold atoms are Al. The grey atoms sit in positions of magnetic frustration. In (a) these are Fe(II) and in (b) they are Al. The first three layers of the 128-atom cubic unit cells are shown in perspective.

magnetic moments. This applies also for the B2 structure away from stoichiometry.

The appearance of a SDW pattern with wave vectors $\vec{q} = 2\pi(\pm\frac{1}{4}, \pm\frac{1}{4}, \pm\frac{1}{4})/a_0$ would not have been surprising if Fe(43Al) had the cubic Fe_9Al_7 structure, but it does not. [The diffraction pattern shows only weak diffuse intensity at the positions, e.g., $(\frac{1}{2}, \frac{1}{2}, \frac{1}{2})$, where the Fe_3Al ordering would give Bragg peaks.] If n were 8 for the Fe_9Al_7 structure, the magnetization pattern would be that of Fig. 2, where the antinodes of the SDW pattern are at the centers of eight clusters of nine Fe atoms each. This complex pattern has a unit cell with 1024 atoms. If the moment of each Fe atom depends on the strength of the molecular field forcing the SDWs, then the atoms near the center of the eight clusters of nine Fe atoms would have the highest moment and those at the edges of the supercluster would have the lowest moment.

The randomness of occupation by Fe(II) of the Al sublattice precludes the long-range AFM structure of Fig. 2, but an approximation to such a pattern could be maintained by shifting the phase of the pattern with respect to the lattice over the distances of coherence found in the diffraction results. The coherence length is seen in the breadth of the $(\frac{1}{7}, \frac{1}{7}, \frac{1}{7})$ peak in the diffraction pattern of polycrystalline Fe(40Al) shown in Fig. 3(a). There is a decrease in the small-angle neutron scattering from 120 to 1.7 K. The difference between the patterns at these temperatures shows that most of the decrease in scattering intensity reappears as a broadened peak with a periodicity of 1.17 nm and a coherence length of 5 nm. The peak position yields the magnitude of the scattering vector. The single crystals provide the direction; see Fig. 3(b). There is negligible difference in results between the polycrystalline material, a well-characterized homogeneous alloy of remarkable ductility [13], and the single crystal of Fe(40Al). The crystals were grown from the melt using the Bridgeman method [14].

The temperature dependence for the scattering amplitude of the $(\frac{1}{n}, \frac{1}{n}, \frac{1}{n})$ peaks is shown in Fig. 4. There is no obvious sign of the freezing temperatures, known from the ac susceptibility work of Shull *et al.* [7] and Takahashi *et al.* [8]. These data resemble neutron scattering from a weak ferromagnetic material in a large applied field. It matches the behavior of the dynamically fluctuating SDW clusters seen in Cu(Mn), Pd(Mn), and Pd(Cr) spin-glass alloys [15–17], for which greatly refining the energy selection in triple axis neutron spectrometry leads to some resolution of the freezing process.

The solid lines in Fig. 4 describe the response of a localized moment to an applied field plus a cooperative field proportional to the resulting moment. The neutron scattering intensity $I = (\mu_q/\mu_{q0})^2(I_{q0} - I_{BG}) + I_{BG}$, where

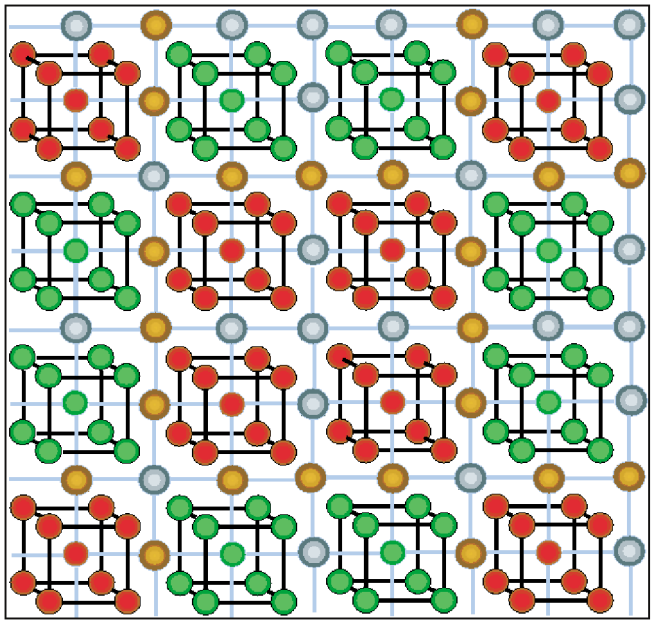

FIG. 2 (color). Magnetization patterns with cubic symmetry for Fe_9Al_7 with the magnetic unit cell doubled in each direction to form a structure that would produce magnetic scattering related to that observed in Fe(43Al) . The first three layers of the 1024-atom unit cell are shown with the coding of Fig. 1.

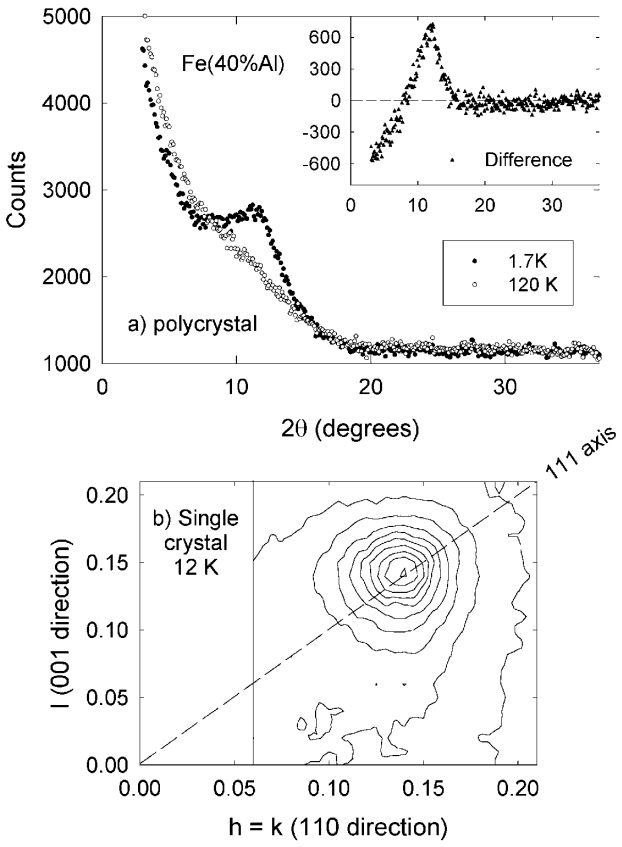

FIG. 3. Neutron scattering intensity for (a) polycrystalline Fe(40Al) at 120 and 1.7 K with their difference shown in the inset and (b) single crystal Fe(40Al) at 12 K shown as contours about the $(\frac{1}{7}, \frac{1}{7}, \frac{1}{7})$ peak.

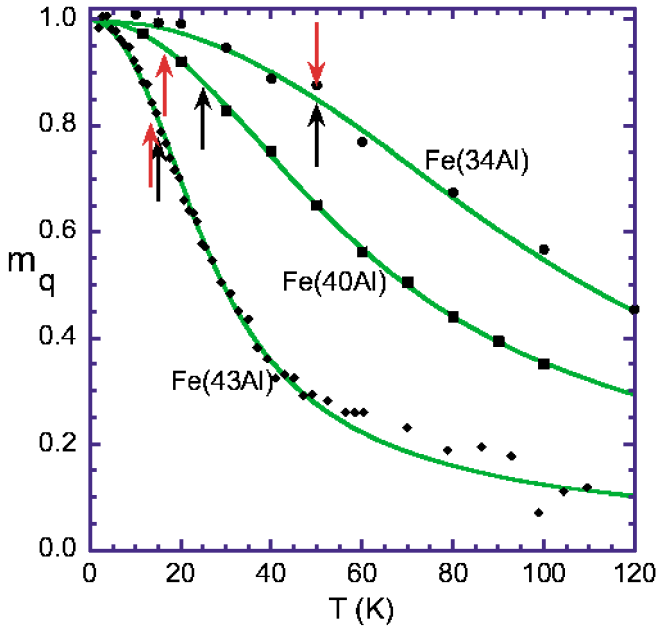

FIG. 4 (color). Temperature dependence of the SDW amplitudes of Fe(Al) single crystals [14]. The black arrows are the freezing temperatures from Ref. [8]. Fitting with Eq. (1) yields the solid curves. The red arrows are the T_Λ from the fits.

μ_q, the moment at wave vector $\vec{q}$, is given implicitly by $m_q \equiv \mu_q/\mu_{q0} = B_J(\mu_{q0}(H_q + \Lambda_q\mu_q)/k_BT)$, where B_J is the Brillouin function. The relation between T and m_q is simplified by using the approximation $B_3(x) \cong 1/\sqrt{[(9/4x)^2 + 1]}$ to give

$$T = (T_H/m_q + T_\Lambda)\sqrt{(1 - m_q^2)}. \quad (1)$$

The fitting yields estimates of $T_\Lambda \equiv \Lambda_q\mu_{q0}^2/k_B$ and $T_H \equiv \mu_{q0}H_q/k_B$. T_Λ is a measure of the cooperative interaction of the Fe moments. T_H is a measure of the strength of H_q. These are compared in Table I with the freezing temperatures T_f from Takahashi *et al.* [8]. The field H_q is assumed here to be temperature independent. If H_q is interpreted as coming from the spin density waves, this implies a high value for the Néel temperature of the SDW compared to T_Λ. The SDW field H_q appears to persist far above T_Λ.

The breadth of the SDW peaks, e.g., see Fig. 3, can be interpreted as shifts in the phase of the SDWs with respect to the lattice with the phase changing at the rate of ~0.1 rad/nm. Conceptually there is a difference between a picture where the SDWs have abrupt shifts of phase at domain boundaries or gradual shifts as the SDWs adjust to take into account the positions of the clusters with an Fe(II) atom surrounded by eight Fe(I) atoms. While neutron diffraction cannot distinguish between these, micromagnetic measurements might.

TABLE I. Comparison with freezing temperatures from Takahashi *et al.* [8].

Atomic percent Al	T_f (K)	T_Λ (K)	T_H (K)
34	50	50	38
40	26	17	32
43	15	12	10

Fe(34Al), Fe(40Al), and Fe(43Al) have wave vectors given by $n \sim 11$, ~7, and ~6, respectively, with n increasing with temperature by less than 1 over the range 4 to 120 K. The width of the diffraction peaks also increases with temperature, corresponding to a decrease in coherence length from 5 to 3.5 nm.

In Fe(Al), the eight satellites about the origin appear also around the (1, 1, 0) and (2, 0, 0) reciprocal lattice vectors of the parent bcc lattice, but not around the (1, 0, 0) nor the (1, 1, 1) superlattice reciprocal lattice positions; see Fig. 5. The structures of Figs. 1 and 2 also have eight satellite reflections about each of the reciprocal lattice vectors for the parent bcc structure but not for the superlattice reciprocal lattice positions.

The SDWs in Fe(Al) should be as important to the understanding of magnetism in metals as the SDWs in Cr. In Cr the $\vec{q}$ is just short of $2\pi(1, 0, 0)/a_0$, which makes the moments of nearest neighbors of the bcc structure almost oppositely aligned. This $\vec{q}$ couples states on parallel parts of the Fermi surface to form the SDW. In the iron aluminides, the nearest-neighbor moments are almost aligned parallel. If the principal wave vectors are the 48 combinations of $\vec{q} = 2\pi(\pm(1 + \frac{1}{n}), \pm(1 - \frac{1}{n}), \pm(0 + \frac{1}{n}))/a_0$, these could couple states on opposite sides of the Fermi surface to form the SDWs. Here the wave vectors are in groups of four, each near one of the (1, 1, 0) reciprocal lattice spots of the parent bcc structure; see Fig. 5.

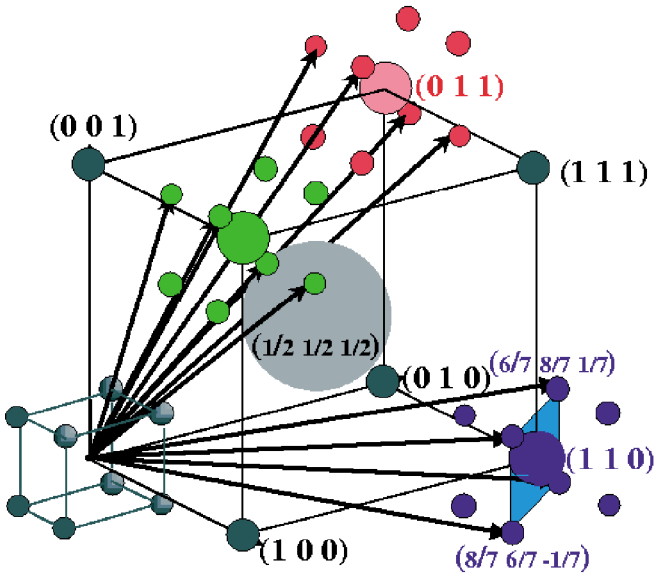

FIG. 5 (color). The reciprocal lattice spots in Fe(40Al).

It is as if each of the 12 (1, 1, 0) wave vectors of the lattice split into four wave vectors that swing away from the (1, 1, 0) to create 48 gaps at the Fermi surface. This suggests the possibility that the application of a high magnetic field could move the wave vectors of the SDW back to the (1, 1, 0), producing field induced ferromagnetism from a commensurate SDW.

From the polycrystalline Fe(40Al) data, we can put a lower bound on the moment per atom if we take as a model the extreme case of a single $\vec{q}$ state with a transverse helical SDW. This yields a moment of $0.26\mu_B$ per atom if every atom (Fe and Al) were to carry the same moment. The decrease in moment with increasing Al, seen in the single crystals, has yet to be quantified.

The competition between near-neighbor FM coupling and third-neighbor AFM coupling through an Al atom has a firm theoretical basis. The superexchange interaction appears in cluster calculations of Reddy *et al.* [18]. Shukla and Wortis [19] obtained spin-glass behavior by remapping the Fe(Al) problem into one that can be treated by renormalization group methods. Grest [12] carried out Monte Carlo calculations with these two specific interactions, obtaining results that mimicked the data of Ref. [7]. Neither of these two studies reproduced the reentrant behavior. The almost ferromagnetic SDWs in Fe(Al) point to another interaction.

The similarities between Fe(Al) and the spin-glass alloys Cu(Mn), Pd(Mn), and Pd(Cr) [15–17] should be noted in this regard. Over 40 years ago Overhauser [20,21] proved that Hartree-Fock theory, which treats exchange as the nonlocal interaction that it is, makes a SDW state lower energy than a paramagnetic state for an electron gas, so-called jellium, when treated rigorously. There is a peak in the wave-vector dependent susceptibility $\chi(\vec{q})$ for wave vectors that span the Fermi surface. Overhauser used this to predict SDWs in Cu(Mn), which were found later. The Cu(Mn) results compel the acceptance of a peak in $\chi(\vec{q})$ [22].

When Overhauser added the corrections to Hartree-Fock theory needed for the correlation energy, he discovered static charge-density-wave (CDW) states with a lower energy than the static SDW states in deformable jellium [23,24]. CDWs have been found recently in liquid $Li(NH_3)_4$ [25].

The SDW and CDW states are closely related [26]. The difference is just a shift in the phase of the static spatial oscillations for spin-up electrons with respect to those for spin-down electrons. In a sufficiently large static field with wave vector $\vec{q}$, the CDW should take on a SDW component. The Fe clusters evident in Figs. 1 and 2 might cause such a phase shift in the (1, 1, 0) CDWs.

CDWs (also called long period superlattices or concentration waves) appear in related B2 alloys of $Ti_{30}V_{20}Al_{50}$, where the wave vectors are quite similar to those observed here [27]. For long period superlattices the connection of the wave vectors to the Fermi surface was firmly established by Sato and Toth [28].

We do not know whether there is indeed cubic symmetry from multiple $\vec{q}$'s in each region or lowered symmetry from single-$\vec{q}$ states in multiple regions. Nothing has been learned yet about polarization axes. We have yet to carry out such tasks as finding the effects of magnetic fields, pressure, strains, and changes in alloy composition by substitution of other atoms. Heat capacity measurements would show whether the moments on the Fe atoms have a thermodynamic spin degree of freedom or result from a more itinerant electron model [29].

This work was supported by U.S. Air Force Office of Scientific Research Grant No. F49620-00-1-0364.

[1] F. Lechermann *et al.*, Phys. Rev. B **65**, 132104 (2002).
[2] G. P. Das *et al.*, Phys. Rev. B **66**, 184203 (2002).
[3] K. Capelle and L. N. Oliveira, Phys. Rev. B **61**, 15 228 (2000).
[4] H. Sato and A. Arrott, Phys. Rev. **114**, 1427 (1959).
[5] S. M. Shapiro, in *Spin Waves and Magnetic Excitations*, edited by A. S. Borovik-Romanov and S. K. Sinha (Elsevier, Amsterdam, 1988), Vol. 2, p. 219.
[6] A. Arrott and H. Sato, Phys. Rev. **114**, 1420 (1959).
[7] R. D. Shull *et al.*, Solid State Commun. **20**, 863 (1976).
[8] S. Takahashi *et al.*, J. Phys. Condens. Matter **8**, 11 243 (1996).
[9] S. J. Pickart and R. Nathans, Phys. Rev. **123**, 1163 (1961).
[10] J. W. Cable *et al.*, Phys. Rev. B **16**, 1132 (1977).
[11] K. Motoya *et al.*, Phys. Rev. B **28**, 6183 (1983).
[12] G. S. Grest, Phys. Rev. B **21**, 165 (1980).
[13] S. C. Deevi, Intermetallics **8**, 679 (2000).
[14] D. Wu and I. Baker, Mater. Sci. Eng. A **329–331**, 334 (2002).
[15] J. W. Cable and Y. Tsunoda, J. Appl. Phys. **73**, 5454 (1993).
[16] F. J. Lamelas *et al.*, Phys. Rev. B **51**, 621 (1995).
[17] Y. Tsunoda *et al.*, Phys. Rev. B **56**, 11 051 (1997).
[18] B. V. Reddy *et al.*, Phys. Rev. B **64**, 132408 (2001).
[19] P. Shukla and M. Wortis, Phys. Rev. B **21**, 159 (1980).
[20] A. W. Overhauser, Phys. Rev. **128**, 1437 (1962).
[21] A. W. Overhauser and G. Lacueva, Phys. Rev. B **66**, 165115 (2002).
[22] O. Fajen and G. Vignale, Solid State Commun. **77**, 829 (1991).
[23] A. W. Overhauser, Phys. Rev. **167**, 691 (1968).
[24] A. W. Overhauser, in *Highlights of Condensed-Matter Theory*, edited by F. Bassani *et al.* (North-Holland, Amsterdam, 1985).
[25] C. A. Burns *et al.*, Phys. Rev. Lett. **86**, 2357 (2001).
[26] A. W. Overhauser, Phys. Rev. B **29**, 7023 (1984).
[27] Gousheng Shao, Appl. Phys. Lett. **74**, 2643 (1999).
[28] H. Sato and R. S. Toth, Phys. Rev. **127**, 469 (1962).
[29] D. A. Papaconstantopoulos *et al.*, J. Appl. Phys. **89**, 6889 (2001).